Highly active CNT-promoted Cu–ZnO–Al_2O_3 catalyst for methanol synthesis from $H_2/CO/CO_2$

Xin Dong, Hong-Bin Zhang *, Guo-Dong Lin, You-Zhu Yuan, and K.R. Tsai

Department of Chemistry & State Key Laboratory of Physical Chemistry for the Solid Surfaces, Xiamen University, Xiamen 361005, China

Received 14 August 2002; accepted 7 November 2002

With types of in-house-synthesized multi-walled carbon nanotubes (CNTs) and the nitrates of the corresponding metallic components, highly active CNT-promoted Cu–ZnO–Al_2O_3 catalysts, symbolized as $Cu_iZn_jAl_k$-x%CNTs, were prepared by the co-precipitation method. Their catalytic performance for methanol synthesis from $H_2/CO/CO_2$ was studied and compared with the corresponding CNT-free co-precipitated catalyst, $Cu_iZn_jAl_k$. It was shown experimentally that appropriate incorporation of a minor amount of the CNTs into the $Cu_iZn_jAl_k$ could significantly increase the catalyst activity for methanol synthesis. Under the reaction conditions of 493 K, 5.0 MPa, $H_2/CO/CO_2/N_2 = 62/30/5/3$ (v/v), GHSV = 8000 h^{-1}, the observed CO conversion and methanol formation rate over a co-precipitated catalyst of $Cu_6Zn_3Al_1$-12.5%CNTs reached 36.8% and 0.291 μmol $CH_3OH\,s^{-1}$ (m^2-surf. Cu)$^{-1}$, which was about 44 and 25% higher than those (25.5% and 0.233 μmol $CH_3OH\,s^{-1}$ (m^2-surf. Cu)$^{-1}$) over the corresponding CNT-free co-precipitated catalyst, $Cu_6Zn_3Al_1$. Addition of a minor amount (10–15 wt%) of the CNTs to the $Cu_6Zn_3Al_1$ catalyst was found to considerably increase specific surface area, especially Cu surface area of the catalyst. H_2-TPD measurements revealed that the CNTs and the pre-reduced CNT-promoted catalyst systems could reversibly adsorb and store a considerably greater amount of hydrogen under atmospheric pressure at temperatures ranging from room temperature to ~573 K. This unique feature would be beneficial for generating microenvironments with higher stationary-state concentration of active hydrogen adspecies on the surface of the functioning catalyst, especially at the interphasial active sites since the highly conductive CNTs might promote hydrogen spillover from the Cu sites to the Cu/Zn interphasial active sites, and thus be favorable for increasing the rate of the CO hydrogenation reactions. Alternatively, the operation temperature for methanol synthesis over the CNT-promoted catalysts can be 15–20 degrees lower than that over the corresponding CNT-free contrast system. This would contribute considerably to an increase in equilibrium CO conversion and CH_3OH yield. The results of the present work indicated that the CNTs could serve as an excellent promoter.

KEY WORDS: carbon nanotubes; $Cu_iZn_jAl_k$-x%CNTs catalysts; methanol synthesis; CO/CO_2 hydrogenation.

1. Introduction

Among the C_1 chemicals, methanol is the species most widely used in various chemical applications. Recently, it has been used as a clean synthetic fuel additive and considered as an alternative fuel source [1]. That methanol is a better and much cleaner automobile fuel with high octane number, and lower emissions of NO_x, ozone, CO, and aromatic vapors has been confirmed by a long-mileage road test carried out in the USA around 1990 [2]. Methanol is also a convenient hydrogen carrier for PEM fuel cells. A recent breakthrough in the conversion of methanol to H_2 via oxidative steam reforming around 500 K is able to produce very pure H_2 with less than a few tens ppm level of CO. H_2 of such high purity can be used directly in H_2–air fuel cells [3].

In existing methanol synthesis technology, only a small portion (~10%) of the syngas feed is converted to methanol, while a larger portion of the unreacted feed, after separation from methanol, must be recycled so as to enhance the utilization ratio of the syngas feed. The process and equipment involved are relatively complicated, and extra energy is consumed for the separation and recycling. Thus, finding more active catalysts and lower-temperature processes with high single-pass conversion of syngas has been one of the key objectives for research and development efforts.

The kinetics and mechanism of the methanol synthesis on Cu–ZnO–Al_2O_3 catalysts have been extensively studied since the late 1970s. A number of studies and excellent review articles have been published on this subject, including those by Klier [4], Kung [5], and Herman [6]. Progress in this field has considerably contributed to the growing understanding of the nature of this catalytic reaction system.

Carbon nanotubes (CNTs) have been drawing increasing attention recently [7]. This type of new carbon material possesses a series of unique features, such as its nanosize channel, the highly conductive graphite-like tube wall, the sp^2-carbon-constructed surface, and its excellent performance with regard to hydrogen adsorption. These features make the CNTs full of promise for being novel catalyst carriers [8–11] or even promoters. We recently reported a type of

* To whom correspondence should be addressed.
E-mail: hbzhang@xmu.edu.cn

1011-372X/03/0200-0237/0

highly active CNT-supported Cu-based catalyst for hydrogenation of CO/CO_2 to methanol [12]. It was experimentally found that the carrier could significantly affect the activity for methanol synthesis. The space-time-yield (STY) of methanol over the CNT-supported catalyst at 503 K was 1.95 and 2.57 times as high as those of the corresponding catalysts supported by AC and γ-Al_2O_3 at their optimum operating temperatures, 523 and 543 K, respectively. In the present work, a series of CNT-promoted Cu–ZnO–Al_2O_3 catalysts was prepared by the co-precipitation method. Their catalytic performance for CO/CO_2 hydrogenation to methanol was studied and compared with that of the corresponding CNT-free conventional co-precipitated Cu–ZnO–Al_2O_3 catalyst. The results shed some light on understanding the nature of promoter action by the CNTs and the prospect of developing highly active catalysts.

2. Experimental

2.1. Catalyst preparation

The CNTs were synthesized by the catalytic method reported previously [13]. The prepared CNTs were a type of multi-walled carbon nanotubes, with O.D. of 10–50 nm and I.D. of ~3 nm. The freshly prepared CNTs were treated with boiling nitric acid for 4 h, followed by rinsing with deionized water, then drying at 473 K under dry nitrogen. Open-end CNTs with somewhat hydrophilic surfaces were then obtained.

A series of CNT-promoted Cu–ZnO–Al_2O_3 catalysts, symbolized as $Cu_iZn_jAl_k$-x%(mass percentage)CNTs, was prepared by the constant pH co-precipitation method [14]. An aqueous solution containing calculated amounts of Cu, Zn, and Al (total equivalent concentration of metallic cations at 4 N), which was prepared by dissolving $Cu(NO_3)_2{\cdot}3H_2O$, $Zn(NO_3)_2{\cdot}6H_2O$, and $Al(NO_3)_3{\cdot}9H_2O$ (all of AR grade) in deionized water, and an aqueous Na_2CO_3 solution (4 N) were simultaneously added dropwise under vigorous stirring into a Pyrex flask containing a calculated amount of the CNTs at constant temperature of 353 K. The addition was adjusted to maintain a constant pH of ~7. The precipitation procedure was completed in 1 h. The precipitate was then continuously stirred for 5 h at a temperature of 353 K, followed by aging overnight at room temperature and then filtering. It was repeatedly rinsed with deionized water until the content of Na^+ ions in the eluant fell below 0.1 ppm as detected by the flame ion absorption method. The precipitate was then dried at 393 K for 4 h and calcined at 543–573 K for 3 h to yield the precursor of the CNT-promoted catalysts. A CNT-free conventional co-precipitated Cu–ZnO–Al_2O_3 catalyst was prepared in a similar way. All samples of catalyst precursor were pressed, crushed, and sieved to a size of 40–80 mesh for the activity evaluation.

2.2. Catalyst evaluation

The catalyst was tested for methanol synthesis in a continuous-flow micro-reactor–GC combination system. An amount of 0.50 g of catalyst (i.e., equivalent to ~0.5 ml of catalyst sample) was used for each test. Prior to the reaction, the catalyst sample was pre-reduced by 5% $H_2 + N_2$ for 16 h. Methanol synthesis from $H_2/CO/CO_2$ over the catalysts was conducted at a stationary state with feed gas composition of $H_2/CO/CO_2/N_2 = 62/30/5/3$ (v/v) under 453–563 K and 2.0 or 5.0 MPa. The reactants and products were determined by on-line GC (Model 102-GD) equipped with a TC detector and dual columns filled with 5A zeolite molecular sieve and 401 porous polymer, respectively. The former column was used for analysis of CO and N_2 (as internal standard), and the latter for CH_3OH, CO/N_2, CO_2, MF, and DMC. CO conversion was calculated by an internal standard analysis method, and methanol formation rate was evaluated by an external standard (i.e., working curve) method.

2.3. Catalyst characterization

BET specific surface area (SSA) of the CNT sample and the catalyst precursors was measured by N_2 adsorption using a Sorptomatic-1900 (Carlo Erba) system. TEM observations were performed using a JEOL JEM-100CX transmission electron microscope. X-ray diffraction measurements were carried out using a Rigaku Rotaflex D/Max-C X-ray diffractometer with CuKα radiation at a scanning rate of $8^\circ\,min^{-1}$. XPS measurements were done using a VG Esca Lab MK-2 system with MgKα radiation (10 kV, 20 mA, $h\nu = 1253.6$ eV) under UHV (10^{-7} Pa), calibrated internally by the Al(2p) binding energy (BE) at 73.6 eV and the carbon deposit C(1s) BE at 284.6 eV.

Tests of H_2-TPR and H_2-TPD of the catalyst were conducted using a fixed-bed continuous-flow micro-reactor or adsorption–desorption system. A KOH column and a 3A zeolite molecular sieve column were installed in sequence at the reactor exit to remove water vapor formed by the reduction of metallic oxide components of the catalyst sample. The rate of temperature increase was $10\,K\,min^{-1}$. Change of hydrogen signal was monitored using on-line GC (Shimadzu GC-8A) with a TC detector. For TPR measurements, 20 mg of catalyst sample was used for each test. The sample was first flushed by an Ar (of 99.999% purity) stream at 673 K for 30 min to clean its surface, and then cooled down to room temperature, followed by switching to a N_2-carried 5 vol% H_2 gaseous mixture as reducing gas to start the TPR observation. For TPD tests, 200 mg of catalyst sample was used each time. Prior to TPD measurement, the catalyst sample was pre-reduced *in situ* in the TPD equipment by a N_2-carried 5 vol% H_2 gaseous mixture, with the highest

reduction temperature reaching 483 K and lasting 16 h. Shortly after, the reduced sample was cooled to 433 K, followed by switching to a H_2 (of 99.999% purity) stream and maintaining at that temperature for 30 min, subsequently cooling down to room temperature and maintaining at room temperature for 1 h, and then flushing by an Ar (of 99.999% purity) stream at room temperature until the stable baseline of GC appeared.

Determination of the metal Cu surface area (Cu-SA) of the catalyst was carried out according to the improved method suggested by Bond and Namuo [15]. The above TPR apparatus was modified to allow flows of (1) 5% H_2 (of 99.999% purity) in N_2 (of 99.999% purity), (2) Ar (of 99.999% purity), and (3) N_2O (of 99% purity, obtained from Aldrich Chemical Co.) to pass sequentially through the reactor and detector. A normal TPR was first performed on a calcined sample in the temperature region 293–593 K, which provided an estimate on the Cu content and produced a reduced catalyst in a suitable state for reaction with N_2O. The heating rate was $10\,K\,min^{-1}$ and the flow rate of the N_2-carried 5% H_2 gaseous mixture was $50\,ml\,min^{-1}$. The reduced sample was then cooled to the reaction temperature of 333 K in the Ar stream, and after 30 min the N_2O was allowed to flow over the sample for 1 h at that temperature at a flow rate of $85\,ml\,min^{-1}$. The N_2O flow was then replaced by Ar and the sample cooled to room temperature. Finally, the 5% $H_2 + N_2$ mixture was introduced and a second TPR was performed. A H_2-TPR peak due to the reduction of the adsorbed O atoms was observed. After the second TPR, a further calibration with a dose of H_2 (of 99.999% purity) was carried out, and the number of surface Cu atoms, Cu_S (assuming $O/Cu_S = 0.5$), and also the Cu surface area (assuming 1.47×10^{19} atoms m^{-2}) was thus calculated.

3. Results and discussion

3.1. Reaction activity of methanol synthesis over the $Cu_iZn_jAl_k$-x%CNTs catalysts

Investigation of the effect of the feed gas GHSV on the reactivity of methanol synthesis over the CNT-promoted catalysts showed that at 2.0 MPa and a certain temperature (e.g. 493 K), CO conversion increased with increasing GHSV from zero to $\sim 3000\,h^{-1}$, and reached a maximum at GHSV close to $3000\,h^{-1}$. It then started to decrease with further increase of GHSV. It was believed that, as the GHSV approached $3000\,h^{-1}$, the reaction of methanol formation was in the kinetics-controlled region. In the present work, reactivity tests of methanol synthesis were performed under the reaction condition of $GHSV = 3000\,h^{-1}$, unless otherwise specified.

It is well known that CO_2 in the feed gas is a participating component indispensable to continuously fast conversion of the syngas to methanol. However, the net conversion of CO_2 indicated by GC analysis of the inlet and exit gases of the reactor was quite low, and all the assay results of the catalyst activity in the present work are shown with CO conversion and methanol formation rate.

Figure 1 shows the assay results of reactivity of methanol synthesis at 453–523 K over the catalysts with different CNT percentages, $Cu_6Zn_3Al_1$-x%CNTs. On all four catalysts, both the CO conversion and the methanol formation rate first went up with increasing temperature, reached a maximum at their respective optimum operating temperature, and then went down as the temperature increased further. This strongly indicated that at the lower temperature range before the

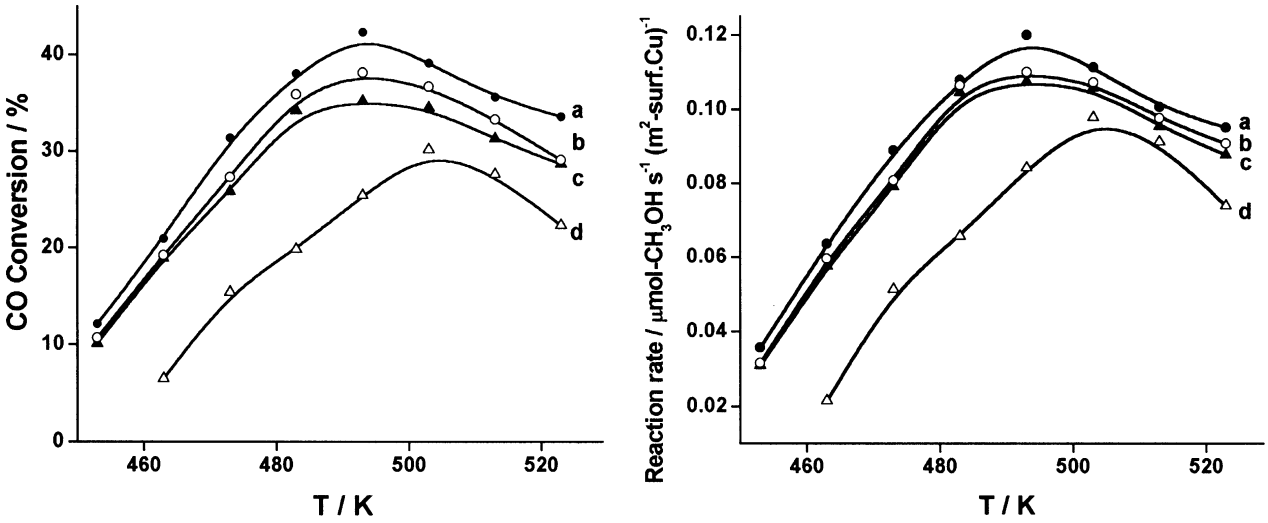

Figure 1. CO conversion and CH_3OH formation rate at different reaction temperatures over a series of catalysts: (a) $Cu_6Zn_3Al_1$-12.5%CNTs; (b) $Cu_6Zn_3Al_1$-10.0%CNTs; (c) $Cu_6Zn_3Al_1$-15.0%CNTs; (d) $Cu_6Zn_3Al_1$-0%CNTs. Reaction conditions: 2.0 MPa, $H_2/CO/CO_2/N_2 = 62/30/5/3$ (v/v), $GHSV = 3000\,h^{-1}$.

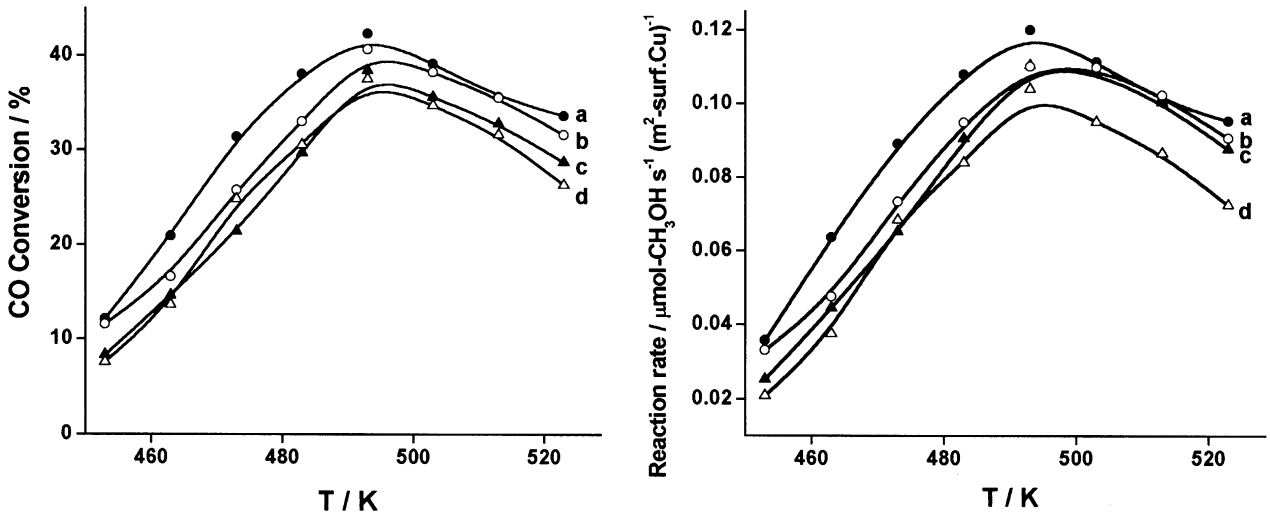

Figure 2. CO conversion and CH_3OH formation rate at different reaction temperatures over a series of catalysts: (a) $Cu_6Zn_3Al_1$-12.5%CNTs; (b) $Cu_5Zn_{2.5}Al_1$-12.5%CNTs; (c) $Cu_4Zn_2Al_1$-12.5%CNTs; (d) $Cu_7Zn_3.5Al_1$-12.5%CNTs. Reaction conditions: 2.0 MPa, $H_2/CO/CO_2/N_2 = 62/30/5/3$ (v/v), GHSV = 3000 h^{-1}.

maximum, the methanol synthesis reaction was controlled by kinetics, and after the maximum, the reaction became equilibrium limited due to the high reaction temperature. The activity sequence observed on these catalysts for methanol synthesis is: (a) $Cu_6Zn_3Al_1$-12.5%CNTs > (b) $Cu_6Zn_3Al_1$-10.0%CNTs > (c) $Cu_6Zn_3Al_1$-15.0%CNTs > (d) $Cu_6Zn_3Al_1$-0.0%CNTs. The optimal value of the CNT percentage seemed to be ~12.5%. Over the $Cu_6Zn_3Al_1$-12.5%CNTs catalyst under the reaction conditions of 493 K, 2.0 MPa, feed gas $H_2/CO/CO_2/N_2 = 62/30/5/3$ (v/v), GHSV = 3000 h^{-1}, CO conversion reached 42.4%, with the corresponding methanol formation rate at 0.118 μmol $CH_3OH\,s^{-1}$ (m^2-surf. Cu)$^{-1}$. In comparison, the values only reached 29.5% and 0.095 μmol $CH_3OH\,s^{-1}$ (m^2-surf. Cu)$^{-1}$, respectively, over the CNT-free corresponding catalyst prepared in the same manner, $Cu_6Zn_3Al_1$, at its optimal operating temperature of 503 K.

Figure 2 shows the assay results of reactivity of methanol synthesis at 453–523 K over the 12.5%CNT-promoted catalysts with different compositions of Cu/Zn/Al (molar ratio). The observed activity sequence of those catalysts for methanol synthesis was: (a) $Cu_6Zn_3Al_1$-12.5%CNTs > (b) $Cu_5Zn_{2.5}Al_1$-12.5%CNTs ≥ (c) $Cu_4Zn_2Al_1$-12.5%CNTs > (d) $Cu_7Zn_{3.5}Al_1$-12.5%CNTs. Over the catalyst with optimal molar ratio of Cu/Zn/Al = 6/3/1, $Cu_6Zn_3Al_1$-12.5%CNTs, CO conversion reached 42.3%, with the methanol formation rate at 0.118 μmol $CH_3OH\,s^{-1}$ (m^2-surf. Cu)$^{-1}$, under the reaction conditions of 2.0 MPa, 493 K, $H_2/CO/CO_2/N_2 = 62/30/5/3$ (v/v), GHSV = 3000 h^{-1}. The corresponding CH_3OH selectivity reached 98.0% and above in the products.

In order to evaluate the performance of the catalysts under working conditions with a higher extent of reaction, the synthesis reaction of methanol from syngas was conducted at higher pressure and GHSV. The results are shown in figure 3. Under the reaction conditions of 493 K, 5.0 MPa, $H_2/CO/CO_2/N_2 = 62/30/5/3$ (v/v) and GHSV = 8000 h^{-1}, methanol formation rate reached 0.291 μmol $CH_3OH\,s^{-1}$ (m^2-surf. Cu)$^{-1}$ over the $Cu_6Zn_3Al_1$-12.5%CNTs catalyst, which was about 25% higher than that (0.233 μmol $CH_3OH\,s^{-1}$ (m^2-surf. Cu)$^{-1}$) over the corresponding CNT-free system, $Cu_6Zn_3Al_1$. Figure 4 shows the operation stability of this catalyst for methanol synthesis lasting 250 h under reaction conditions of 493 K, 5.0 MPa, $H_2/CO/CO_2/N_2 = 62/30/5/3$ (v/v) and GHSV = 8000 h^{-1}, without obvious deactivation of the catalyst observed. The results of the activity assay and the SSA/Cu-SA determinations

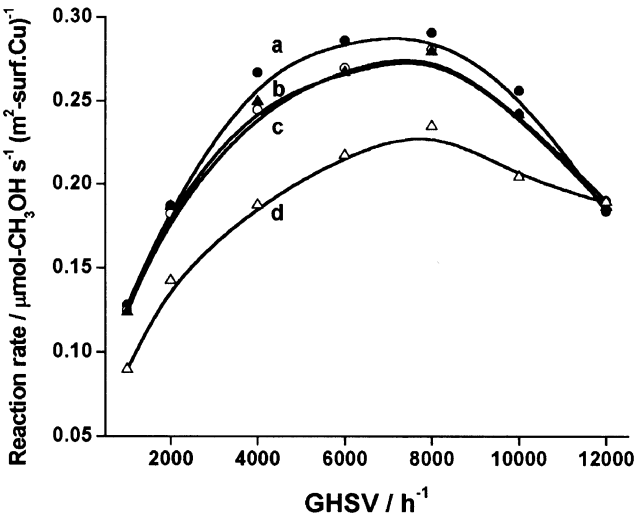

Figure 3. Change of CH_3OH formation rate with GHSV of the feed gas over a series of catalysts: (a) $Cu_6Zn_3Al_1$-12.5%CNTs; (b) $Cu_6Zn_3Al_1$-10.0%CNTs; (c) $Cu_6Zn_3Al_1$-15.0%CNTs; (d) $Cu_6Zn_3Al_1$-0%CNTs. Reaction conditions: 493 K, 5.0 MPa, $H_2/CO/CO_2/N_2 = 62/30/5/3$ (v/v).

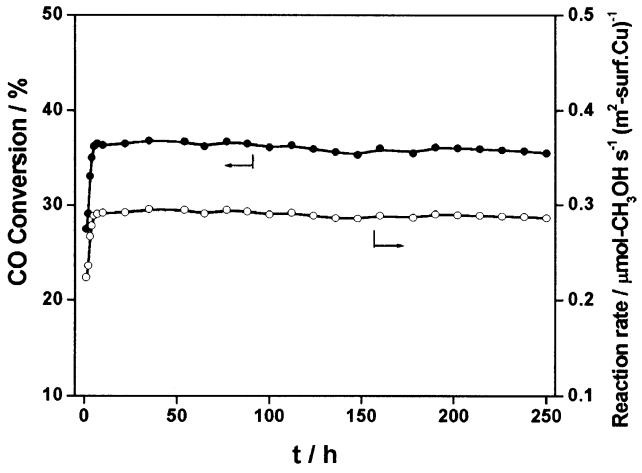

Figure 4. Operation stability of CH_3OH synthesis over the catalyst of $Cu_6Zn_3Al_1$-12.5%CNTs lasting 250 h. Reaction conditions: 493 K, 5.0 MPa, $H_2/CO/CO_2/N_2 = 62/30/5/3$ (v/v), GHSV = 8000 h^{-1}.

of a series of $Cu_iZn_jAl_k$-x%CNTs catalysts for methanol synthesis are summarized in table 1.

3.2. Physicochemical properties of the CNTs as promoter

It is quite evident that the considerably better performance of the CNT-promoted catalysts for methanol synthesis from $H_2/CO/CO_2$ is closely related to the unique structures and properties of the CNTs as promoter. TEM and SEM observations showed that CNTs were almost the only species in the purified CNT products. Elemental analysis showed no other elements than carbon. Figure 5 shows the TEM and SEM images of the CNTs grown from catalytic decomposition of CH_4. These CNTs were uniform in diameter along the tube length with outer diameters in the range 10–50 nm. The HRTEM observation demonstrated that those CNTs derived from CH_4 were constructed by a superposition of many graphene layer facets, which were tilted at a certain angle with respect to the axis of the central hollow nanofiber, as if a number of cones were placed one on top of another [13,16].

The XRD pattern of the CNTs (figure 6(b)) was close to that of graphite (figure 6(a)), but the strongest 002 peak was weakened and somewhat broadened, and the peak position shifted to $2\theta = 26.1^\circ$ from $2\theta = 26.5^\circ$ for graphite, which corresponded to an increase in the spacing between the sp^2 carbon layers from 0.336 nm for graphite to 0.341 nm for the CNTs. The half-peak width was enlarged from $\sim 0.50^\circ$ for graphite to $\sim 1.43^\circ$ for the CNTs, indicating that the degree of long-range order of these nanostructures was lower than that of graphite. On the other hand, the 100 and 004 reflections of the CNTs were considerably enhanced in comparison with those of graphite, implying that their 100 and 004 faces were more exposed.

The spectra of O_2-TPO (temperature-programmed oxidation, with a He-carried 5 vol% O_2 gaseous mixture as oxidant) showed that the carbon nanostructures in the CNT sample were predominantly graphite-like (with the corresponding main oxidation peak at 960–1000 K). The content of amorphous carbon (the corresponding oxidation peak at around 700 K) was very low (less than 10% estimated).

It was known from the BET measurements with N_2 as adsorbate that the specific surface area of this type of CNTs was $\sim 140\ m^2\ g^{-1}$. The size of their inner diameter

Table 1
Reactivity of CH_3OH synthesis from syngas over a series of the CNTs-promoted catalysts $Cu_iZn_jAl_k$-x%CNTs [a]

Catalyst sample	SSA [m^2 (g-catal.)$^{-1}$]	Cu-SA [m^2 (g-catal.)$^{-1}$]	Reaction temperature (K)	CO conversion (%)	Methanol formation rate [μmol $CH_3OH\ s^{-1}$ (m^2-surf. Cu)$^{-1}$]
$Cu_6Zn_3Al_1$-15.0%CNTs	60.3	35.5	453	10.7	0.031
			493	35.1	0.109
$Cu_6Zn_3Al_1$-10.0%CNTs	60.2	36.8	453	11.9	0.031
			493	38.1	0.113
$Cu_6Zn_3Al_1$-12.5%CNTs	61.4	39.4	453	14.1	0.036
			493	42.4	0.118
			493 [b]	36.8 [b]	0.291 [b]
$Cu_6Zn_3Al_1$-0.0%CNTs	50.3	33.9	463	6.5	0.021
			493	25.3	0.082
			503	29.5	0.095
			493 [b]	25.5 [b]	0.233 [b]
$Cu_5Zn_{2.5}Al_1$-12.5%CNTs	55.7	38.3	453	11.6	0.033
			493	39.8	0.114
$Cu_4Zn_2Al_1$-12.5%CNTs	54.2	36.0	453	8.3	0.025
			493	37.5	0.114
$Cu_7Zn_{3.5}Al_1$-12.5%CNTs	62.6	39.9	453	7.6	0.021
			493	36.5	0.100

[a] Reaction conditions: 2.0 MPa, $H_2/CO/CO_2/N_2 = 62/30/5/3$ (v/v), GHSV = 3000 h^{-1}.
[b] Data at 5.0 MPa and GHSV = 8000 h^{-1}.

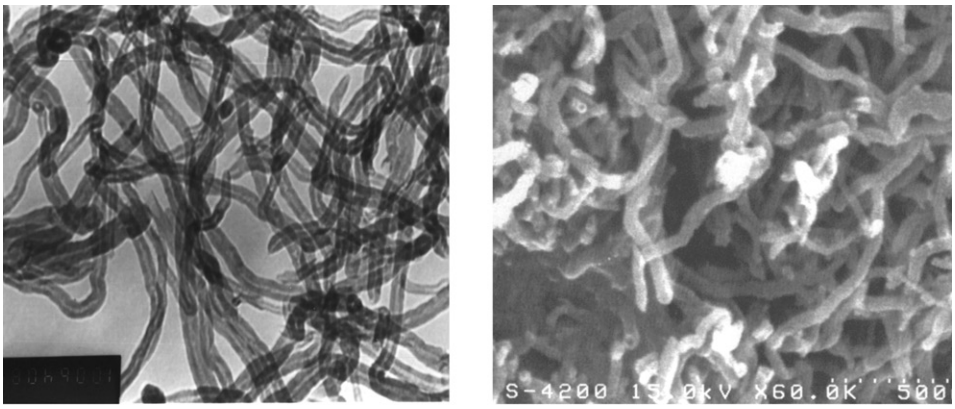

Figure 5. (a) TEM and (b) SEM images of the CNTs grown catalytically by CH_4 decomposition.

was in the range 2.6–3.4 nm, which is consistent with that estimated from the HRTEM image [13,16].

3.3. TPR and TPD/TPSR characterization of the catalysts

The H_2-TPR spectra of the oxidation precursors of the catalysts are shown in figure 7. The H_2 reduction of $Cu_6Zn_3Al_1$-12.5%CNTs sample started at ~453 K and the main TPR peak appeared at round 508 K. On the CNT-free $Cu_6Zn_3Al_1$ catalyst, apparent reduction by H_2 started at 478 K, and reached a peak value at ~528 K, which was ~20 K higher than that of the 12.5%CNTs-promoted system. The observed reducibility sequence of the four samples was: (a) $Cu_6Zn_3Al_1$-12.5%CNTs > (b) $Cu_6Zn_3Al_1$-10.0%CNTs > (c) $Cu_6Zn_3Al_1$-15.0%CNTs > (d) $Cu_6Zn_3Al_1$-0%CNTs. It is conceivable that a lower reduction temperature would be beneficial to inhibiting the growth of metal Cu crystallite produced by the H_2 reduction, thus favorable to increasing the Cu exposed area, which, in turn, enhances the catalyst activity. The above reducibility sequence was consistent with the sequence of the Cu exposed area of those catalysts and their catalytic activity for methanol synthesis (see table 1).

Figure 8 shows the TPD spectrum taken on the CNT sample adsorbing H_2 (99.999% purity) at room temperature. With increasing temperature, the first main TPD peak was present at ~400 K, followed by a shoulder peak at ~485 K and the second main peak at 990 K. Further investigation by GC and MS indicated that the desorbed product was almost exclusively gaseous hydrogen at temperatures lower than ~693 K. At temperatures higher than ~693 K, the product contained a small amount of CH_4, C_2H_4, and C_2H_2, in addition to a considerable amount of H_2 [17]. This result suggested that H_2 adsorption on this type of CNTs may be in two forms: associative (molecular state) and dissociative (atomic state), as demonstrated by the recent UV–vis Raman spectroscopic investigation of the H_2/CNTs adsorption system, for which Raman peaks at 3950, 2856, and 2967 cm^{-1} assignable to H–H stretch of

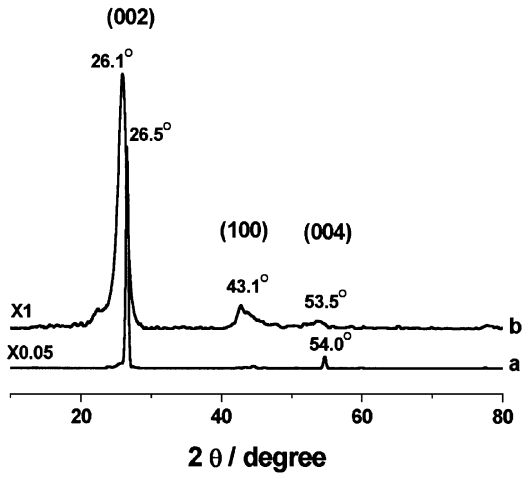

Figure 6. XRD patterns of (a) graphite and (b) the CNTs grown catalytically by CH_4 decomposition.

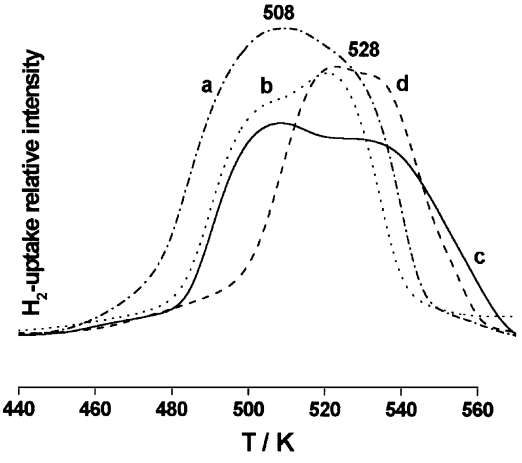

Figure 7. H_2-TPR spectra of the catalyst precursors: (a) $Cu_6Zn_3Al_1$-12.5%CNTs; (b) $Cu_6Zn_3Al_1$-10.0%CNTs; (c) $Cu_6Zn_3Al_1$-15.0%CNTs; (d) $Cu_6Zn_3Al_1$-0%CNTs.

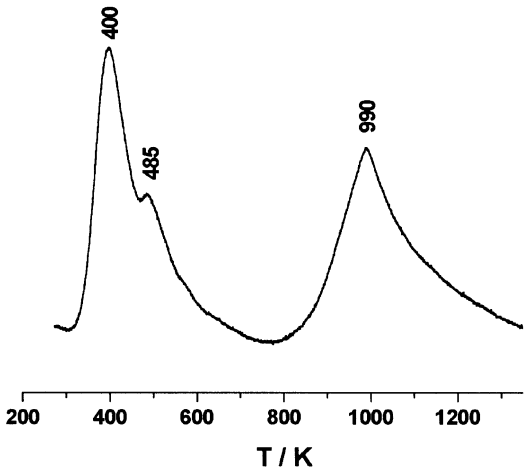

Figure 8. TPD spectrum of the CNTs adsorbing H_2 at room temperature.

molecularly adsorbed H_2(a), symmetric C–H stretch of surface CH_2, and asymmetric C–H stretch of surface CH_3 (both originated from dissociative adsorption of H_2 on the CNTs), respectively, were observed [18].

Figure 9 shows the TPD spectra of H_2 adsorbed at 433 K followed by cooling down to room temperature on the pre-reduced catalysts. Overall, each spectrum contained a lower-temperature peak (peak I) centered round 383 K and a higher-temperature peak (peak II) spanning from 453 to 773 K or higher. The lower-temperature peaks resulted from the desorption of weakly adsorbed species, most probably molecularly adsorbed hydrogen H_2(a), and the higher-temperature peaks were attributed to the desorption of strongly adsorbed species, perhaps dissociatively adsorbed hydrogen H(a). The relative area-intensities of peak Is and peak IIs for these catalyst samples were estimated, and the results are shown in table 2. It is conceivable that at the temperatures for methanol synthesis (453–563 K for the present work), the surface concentration of hydrogen adspecies associated with peak I was expected to be very low, and most of

Table 2
Relative area-intensity of H_2-TPD peaks I and II for the $Cu_6Zn_3Al_1$-x%CNTs catalysts

Catalyst sample	Relative area-intensity [a]	
	Peak I	Peak II
$Cu_6Zn_3Al_1$-12.5%CNTs	42	100
$Cu_6Zn_3Al_1$-10.0%CNTs	33	82
$Cu_6Zn_3Al_1$-15.0%CNTs	32	74
$Cu_6Zn_3Al_1$-0%CNTs	14	43

[a] With area-intensity of the strongest peak II as 100.

hydrogen adspecies at the surface of the functioning catalysts corresponded to peak II. It was probably those strongly adsorbed H species that were closely associated with the reaction activity of methanol synthesis. The ratio of relative area-intensities of peak IIs for these catalysts was: ($Cu_6Zn_3Al_1$-12.5%CNTs)/($Cu_6Zn_3Al_1$-10.0%CNTs)/($Cu_6Zn_3Al_1$-15.0%CNTs)/($Cu_6Zn_3Al_1$-0%CNTs) = 100/82/74/43 (see table 2). This suggested that the sequence of increasing surface concentration of hydrogen adspecies at the functioning catalysts was: $Cu_6Zn_3Al_1$-12.5%CNTs > $Cu_6Zn_3Al_1$-10.0%CNTs > $Cu_6Zn_3Al_1$-15.0%CNTs > $Cu_6Zn_3Al_1$-0%CNTs, in line with the observed sequence of catalytic activity of these catalysts for methanol synthesis.

With CO (99.999% purity) in place of H_2 as adsorbate in the above experiments, the obtained CO-TPD spectra are shown in figure 10. Each of these spectra has three peaks, i.e., peak I at ~393 K, peak II at 468–473 K, and peak III at 543–558 K. The relative area-intensities of these peaks were estimated and are listed in table 3. It is well known that there exist three kinds of sites for CO adsorption at the surface of copper–zinc oxide catalyst for methanol synthesis: Cu^+, Cu^0, and Zn^{2+}, and only Cu^+ species were known to adsorb CO strongly [19]. Thus, the observed low-temperature peaks (peak Is)

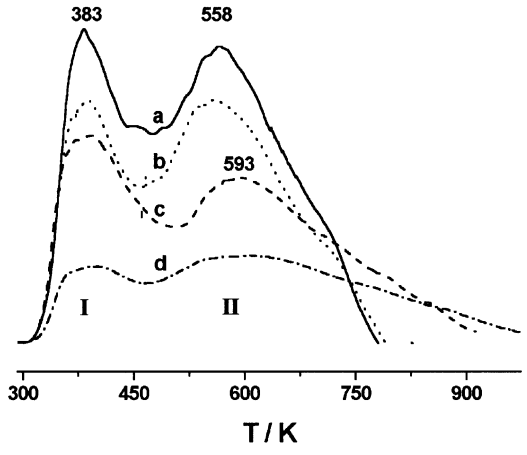

Figure 9. TPD spectra of hydrogen adsorbed on the pre-reduced catalysts: (a) $Cu_6Zn_3Al_1$-12.5%CNTs; (b) $Cu_6Zn_3Al_1$-10.0%CNTs; (c) $Cu_6Zn_3Al_1$-15.0%CNTs; (d) $Cu_6Zn_3Al_1$-0%CNTs.

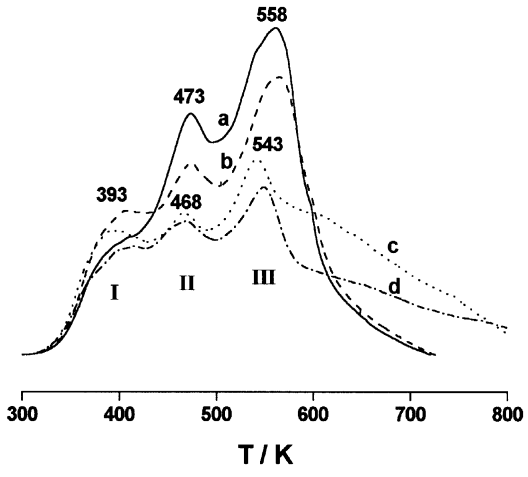

Figure 10. TPD spectra of CO adsorbed on the pre-reduced catalysts: (a) $Cu_6Zn_3Al_1$-12.5%CNTs; (b) $Cu_6Zn_3Al_1$-10.0%CNTs; (c) $Cu_6Zn_3Al_1$-15.0%CNTs; (d) $Cu_6Zn_3Al_1$-0%CNTs.

Table 3
Relative area-intensity of CO-TPD peaks I, II, and III for the $Cu_6Zn_3Al_1$-x%CNTs catalysts

Catalyst sample	Relative area-intensity [a]		
	Peak I	Peak II	Peak III
$Cu_6Zn_3Al_1$-12.5%CNTs	27	46	100
$Cu_6Zn_3Al_1$-10.0%CNTs	31	41	90
$Cu_6Zn_3Al_1$-15.0%CNTs	27	28	85
$Cu_6Zn_3Al_1$-0%CNTs	23	25	60

[a] With area-intensity of the strongest peak III as 100.

could be reasonably attributed to desorption of weakly adsorbed CO species, most likely non-dissociatively adsorbed CO species on Zn^{2+} sites. The higher-temperature peaks (peak IIs and IIIs) corresponded to desorption of medium-to-strongly and strongly adsorbed CO species, most likely non-dissociatively adsorbed CO species on Cu^0 and Cu^+ sites, respectively. Additional evidence in supporting these assignments also came from the experimental fact that the area-intensity sequence of peak IIs and IIIs of these catalyst samples (see table 3) was in keeping with the sequence of their Cu exposed area (see table 1), i.e., $Cu_6Zn_3Al_1$-12.5%CNTs > $Cu_6Zn_3Al_1$-10.0%CNTs > $Cu_6Zn_3Al_1$-15.0%CNTs > $Cu_6Zn_3Al_1$-0%CNTs, while the area-intensity sequence of peak Is was not.

Conceivably, at the temperatures for the methanol synthesis reaction (453–563 K for the present work), the surface concentration of weakly adsorbed CO species associated with peak I was expected to be very low, and most CO adspecies at the surface of the functioning catalyst were those associated with peak II, especially peak III. Most likely it was those strongly adsorbed CO species that were related to the reaction activity of methanol synthesis. It was evident that the incorporation of a minor amount of the CNTs into $Cu_6Zn_3Al_1$ led to a significant increase of the surface active sites for CO adsorption due to its increasing the Cu exposed area of the catalyst, which would be conducive to increasing the concentration of adsorbed CO species on the surface of the functioning catalyst, and thus to enhancing the reaction rate of methanol synthesis.

Using the feed gas of $H_2/CO/CO_2 = 62/30/5$ (v/v) in place of H_2 or CO as adsorbate in the above experiments, the observed TPD-TPSR (temperature-programmed surface reaction) spectra are shown in figure 11. On the sample of $Cu_6Zn_3Al_1$-12.5%CNTs pre-adsorbing the feedgas of $H_2/CO/CO_2$, a main peak at ~451 K and a shoulder peak at ~523 K were observed. The desorbed product was mainly H_2 and CO at temperatures below 453 K. It contained methanol in addition to H_2 and CO at temperatures of 453 K and above. With temperature increasing and the surface reaction speeding up, most of the adspecies of H_2, CO, and CO_2 remaining at the surface may be converted to methanol, which

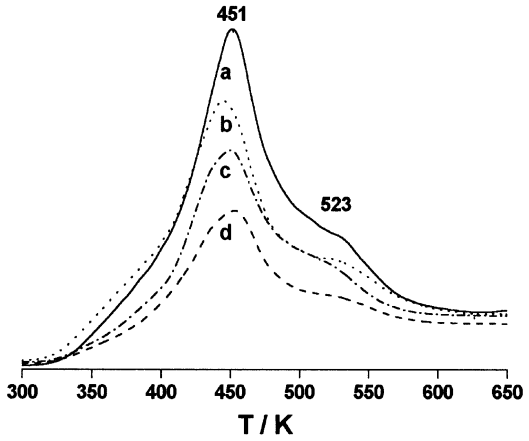

Figure 11. TPD-TPSR spectra of syngas ($H_2/CO/CO_2$) adsorbed on the pre-reduced catalysts: (a) $Cu_6Zn_3Al_1$-12.5%CNTs; (b) $Cu_6Zn_3Al_1$-10.0%CNTs; (c) $Cu_6Zn_3Al_1$-15.0%CNTs; (d) $Cu_6Zn_3Al_1$-0%CNTs.

was easy to desorb, so that the whole process of TPD-TPSR came to an end with the temperature reaching ~600 K. Similar TPD-TPSR behavior was also observed on the other three co-precipitated catalysts, but their adsorption capacities of the feed syngas of $H_2/CO/CO_2$ were relatively low, especially on the CNT-free catalyst, $Cu_6Zn_3Al_1$. The observed sequence of adsorption capacity of these catalysts toward the feed syngas of $H_2/CO/CO_2$ is: $Cu_6Zn_3Al_1$-12.5%CNTs > $Cu_6Zn_3Al_1$-10.0%CNTs > $Cu_6Zn_3Al_1$-15.0%CNTs > $Cu_6Zn_3Al_1$-0%CNTs, again in line with the observed sequence of their catalytic activity for methanol synthesis.

3.4. XRD and XPS characterization of the catalysts

Figure 12 shows the XRD patterns of the CNT-free $Cu_6Zn_3Al_1$ and $Cu_6Zn_3Al_1$-12.5%CNTs systems in the different chemical states. For the CNT-containing

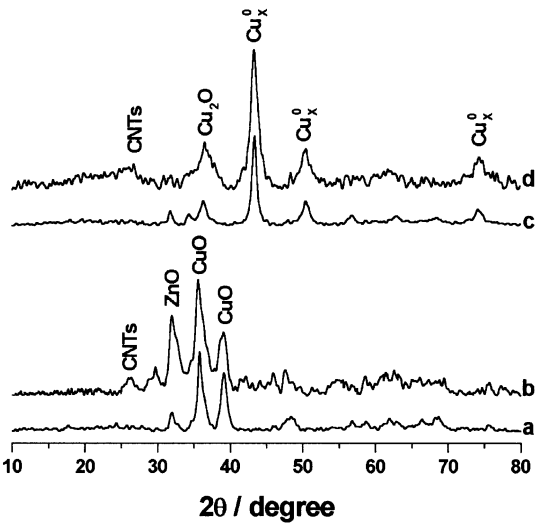

Figure 12. XRD patterns of (a) $Cu_6Zn_3Al_1$ and (b) $Cu_6Zn_3Al_1$-12.5%CNTs both in the oxidation state; (c) $Cu_6Zn_3Al_1$ and (d) $Cu_6Zn_3Al_1$-12.5%CNTs both in the functioning state.

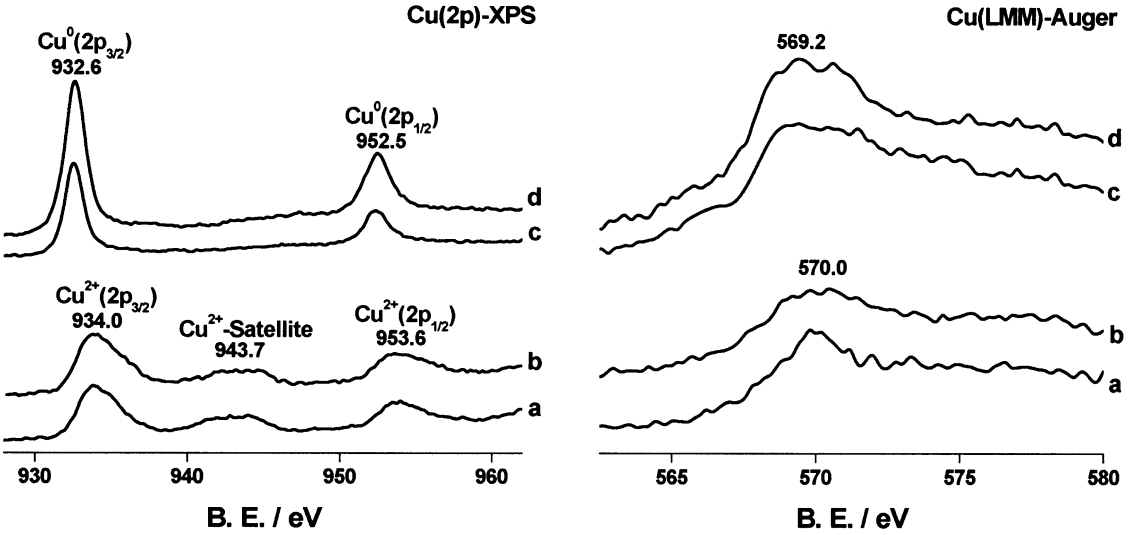

Figure 13. Cu(2p) XPS–Auger spectra of (a) $Cu_6Zn_3Al_1$ and (b) $Cu_6Zn_3Al_1$-12.5%CNTs both in the oxidation state; (c) $Cu_6Zn_3Al_1$ and (d) $Cu_6Zn_3Al_1$-12.5%CNTs both in the functioning state.

system in the oxidation state or in the functioning (reduction) state after 5 h of operating for the methanol synthesis, the graphite-like feature due to the CNTs appeared at $2\theta = 26.1^\circ$ (see figures 12(b) and (d)), in keeping with the CNT feature shown in figure 6(b). The features at $2\theta = 35.8^\circ$ and 39.5° ascribed to CuO phase could be easily identified for the two oxidized samples (figures 12(a) and (b)). On the two samples in the functioning state, strong Cu^0 phase peaks ($2\theta = 43.2^\circ$, 50.4°, and 74.4°) and a relatively weak Cu_2O peak ($2\theta = 36.4^\circ$) were simultaneously observed (figures 12(c) and (d)), indicating that major amounts of the Cu species were in the metal Cu^0 phase and minor amounts in the Cu_2O phase in the functioning catalysts.

The XPS–Auger measurements provide direct experimental evidence about the valence states of the Cu species at the surface of the catalyst. On the oxidized samples of CNT-free $Cu_6Zn_3Al_1$ and $Cu_6Zn_3Al_1$-12.5%CNTs, $Cu^{2+}(2p_{3/2}/2p_{1/2})$ XPS peaks appeared at 934.0/953.6 eV (BE), with the corresponding Cu^{2+} satellite peak and $Cu(L_3M_{45}M_{45})$ Auger peak at 943.7 and 570.0 eV (BE), respectively (see figures 13(a) and (b)). At the surface of the functioning catalysts after 5 h of operating for the methanol synthesis, Cu^0 was the dominant Cu species, with $Cu^0(2p_{3/2}/2p_{1/2})$ at 932.6/952.5 eV (BE) and $Cu^0(L_3M_{45}M_{45})$ at 569.2 eV (BE) (see figures 13(c) and (d)) [20]. The surface concentration of Cu^+ was under the XPS detection limit, even though a minor amount of Cu_2O crystallite was observed in the XRD measurements (see figures 12(c) and (d)).

From figures 12 and 13, it can be seen that the XRD pattern and Cu(2p) XPS–Auger spectra of the CNT-promoted system, $Cu_6Zn_3Al_1$-12.5%CNTs, were quite close to those of the CNT-free contrast system, $Cu_6Zn_3Al_1$, in the position and shape as well as relative intensity of the features associated with the Cu component. It appears that the doping of a minor amount of the CNTs into $Cu_6Zn_3Al_1$ did not lead to significant change in the phase composition of the Cu component in the functioning catalyst and in the relative concentrations of catalytically active Cu species with different valence states at the functioning catalyst surface.

3.5. Nature of the CNT promoter action

The results of the BET specific surface area and Cu surface area measurements shown in table 1 indicated that the doping of a minor amount of the CNTs led to a considerable increase in specific surface area (SSA) and Cu surface area (Cu-SA) of the catalyst. For the $Cu_6Zn_3Al_1$-12.5%CNTs catalyst, a 22% increase of specific surface area and a 16% increase of Cu surface area were observed as compared with those of the catalyst $Cu_6Zn_3Al_1$. The increment of specific surface area, especially Cu surface area, was undoubtedly in favor of enhancing the specific activity of the catalysts (i.e., activity of unit mass of catalyst). Nevertheless, it would be difficult to believe that the increase of as high as 44% of CO conversion (i.e., 36.8% vs. 25.5% for the $Cu_6Zn_3Al_1$-12.5%CNTs and the CNT-free $Cu_6Zn_3Al_1$, respectively, see table 1) was solely attributed to the difference in their specific surface area and Cu surface area. Besides, the difference in the surface areas could hardly justify the 25% increase of the intrinsic methanol formation rate (i.e., from 0.233 μmol $CH_3OH\,s^{-1}$ $(m^2\text{-surf. Cu})^{-1}$ for the CNT-free $Cu_6Zn_3Al_1$ to 0.291 μmol $CH_3OH\,s^{-1}$ $(m^2\text{-surf. Cu})^{-1}$ for the $Cu_6Zn_3Al_1$-12.5%CNTs).

Thus, it appears that the high reactivity, especially the high intrinsic reaction rate, for methanol synthesis over the CNT-promoted catalyst is closely related to the peculiar structure and properties of the carbon

nanotubes as promoter. From a chemical catalysis point of view, the excellent performance of the CNTs in hydrogen adsorption/storage and electron transport is very attractive, in addition to its high mechanical strength, nanosize channel, sp^2-C-constructed surface, and graphite-like tube wall. It could be inferred from the above TPD/TPSR investigations that there would exist a considerable amount of reversibly adsorbed hydrogen species on the CNT-containing catalyst under the conditions of methanol synthesis used in the present study. This would lead to higher stationary-state concentration of active hydrogen adspecies on the surface of the functioning catalyst, especially at the interphasial active sites since the highly conductive CNTs might promote hydrogen spillover from the Cu sites to the Cu/Zn interphasial active sites, and thus be favorable to increasing the rate of a series of surface hydrogenation reactions in the process of CO/CO_2 hydrogenation to methanol. Alternatively, the operating temperature for methanol synthesis of the catalysts appropriately promoted with a minor amount of CNTs can be 15–20 K lower than that of the corresponding CNT-free contrast system. This would contribute considerably to an increase in equilibrium conversion of CO and yield of CH_3OH. The results of the present study indicated that CNTs could serve as an excellent promoter, and that its unique feature of adsorbing H_2 may play an important role in effectively promoting the methanol synthesis.

In summary, the origins of the promoter action by CNTs in enhancing the reaction activity of the methanol synthesis most likely involve the following aspects:

(a) The CNTs could serve as an excellent dispersant for $Cu–ZnO–Al_2O_3$ components. Proper incorporation of a minor amount of the CNTs into the $Cu_iZn_jAl_k$ significantly increases the Cu exposed area, generating more catalytically active Cu sites at the catalyst surface for CO/CO_2 hydrogenation reaction.
(b) The CNTs could serve as an excellent adsorbent, activator, and reservoir of H_2, which would be beneficial to generating microenvironments with higher stationary-state concentration of active hydrogen adspecies on the surface of the functioning catalyst, and thus favorable to enhancing the rate of the CO/CO_2 hydrogenation reactions.

Further studies on the kinetics and the possible effect of promoting hydrogen spillover are currently under investigation.

Acknowledgments

The authors are grateful for the financial support from National Natural Science Foundation (Project No. 50072021), Education-Ministerial Sci. Foundation (Project No. 99069), and Fujian Provincial Natural Science Foundation (Project No. 2001H017) of China.

References

[1] L.V. MacDougall, Catal. Today 8 (1991) 337.
[2] R.M. Bata, Reprints 207th ACS Meeting (San Diego, 1994); Div. Fuel Chem. 39 (1994) 299.
[3] R.F. Savinell, in: *Proc. Int. Conf. on Applied Electrochemistry* (University of Hong Kong, 1995).
[4] K. Klier, Adv. Catal. 31 (1982) 243.
[5] H.H. Kung, Stud. Surf. Sci. Catal. 45 (1989) 228.
[6] R.H. Herman, Stud. Surf. Sci. Catal. 64 (1991) 265.
[7] K.P. De Jong and J.W. Geus, Catal. Rev. Sci. Eng. 42 (2000) 481.
[8] J.M. Planeix, N. Coustel, B. Coq, V. Brotons, P.S. Kumbhar, R. Dutartre, P. Geneste, P. Bernier and P.M. Ajiayan, J. Am. Chem. Soc. 116 (1994) 7935.
[9] M.S. Hoogenraad, M.F. Onwezen, A.J. van Dillen and J.W. Geus, Stud. Surf. Sci. Catal. 101 (1996) 1331.
[10] Y. Zhang, H.B. Zhang, G.D. Lin, P. Chen, Y.Z. Yuan and K.R. Tsai, Appl. Catal. A: General 187 (1999) 213.
[11] H.B. Zhang, Y. Zhang, G.D. Lin, Y.Z. Yuan and K.R. Tsai, Stud. Surf. Sci. Catal. 130 (2000) 3885.
[12] H.B. Zhang, X. Dong, G.D. Lin, Y.Z. Yuan and K.R. Tsai, Preprints 223rd ACS Meeting (Orlando, 2002); Div. Fuel Chem. 47 (2002) 284.
[13] P. Chen, H.B. Zhang, G.D. Lin, Q. Hong and K.R. Tsai, Carbon 35 (1997) 1495.
[14] P.G. Herman, K. Klier, G.W. Simmons, B.F. Finn, J.B. Bulko and T.P. Kobylinski, J. Catal. 56 (1979) 407.
[15] G.C. Bond and S.N. Namuo, J. Catal. 118 (1989) 507.
[16] P. Chen, H.B. Zhang, G.D. Lin and K.R. Tsai, Chem. J. Chinese Univ. 19 (1998) 765.
[17] Z.H. Zhou, X.M. Wu, Y. Wang, G.D. Lin and H.B. Zhang, Acta Physico-Chemica Sinica (Chinese) 18 (2002) 692.
[18] H.B. Zhang, G.D. Lin, Z.H. Zhou, X. Dong and T. Chen, Carbon 40 (2002) 2429.
[19] Y.Y. Huang, J. Catal. 30 (1973) 187.
[20] S. Marisa, Chem. Phys. Lett. 63 (1979) 52.